An Information Theoretic Analysis on Indoor PLC Channel Characterizations

Hao LIN[*†], Aawatif MENOUNI[†] and Pierre SIOHAN[*]
* France Télécom, Orange Labs, 4, rue du Clos Courtel,
B.P. 91226, 35512 Cesson Sévigné Cedex, France
† Eurecom Institute, 229 route des Crêtes,
B.P. 193, 06904 Sophia Antipolis, France

Abstract—**Power-Line is recently considered as a future medium for the high rate transmissions. But the development of Power Line Communications (PLC) highly depends on the knowledge of the channel characterizations. For this reason, a large number of attentions have been payed on the PLC channel analysis using the measurements. This paper highlights an information theoretic analysis for indoor PLC channel environment investigation, wherein, the estimated channel entropy and the power delay spectrum are expected to give us much useful information to describe the indoor PLC channels. Moreover, the study on the PLC channel degree of freedom distribution and the discussion of choosing whether wide-band or multi-band are included in this paper.**

I. INTRODUCTION

Nowadays, power-line has become a quite attractive medium for the indoor home networks. Its wide-band services in the $2-30$ Mhz frequency band turns out to achieve data transmission rates up to 200 Mb/s [?], whereby, it can be utilized for multi-purposes, e.g. data transmission, home automation products control and internet access. Moreover, the PLC bandwidth is possibly to extend up to 100 Mhz, in order to further increase the data rates. Meanwhile, its lower economic cost also makes economical sense. However, the realization of the access networks requires the PLC technology to provide a satisfying quality of service. To realize so, a study of power-line channel characterizations tends to be mandatory. Although the extensive researches on characterizations of power-line channels have been studied as for instance [?], [?], [?], these studies are mainly focused on frequencies not beyond 30 Mhz.

Recently, the indoor PLC channel measurements were collected by Orange Labs, Lannion [?]. These measurements were undertaken up to 100 Mhz bands in various indoor channel environments (country and urban, new and old, apartments and houses). Further, it turns out that the PLC channels can be classified into 9 classes in terms of their capacities. Later after, a time-frequency analysis based on these measurements was reported in [?], where the estimated coherence bandwidth and RMS delay spread were studied.

In this paper, we aim at investigating the channel characterizations, from an information theory point of view, for these different classes. It shows that the entropy analysis can already give us much useful information on the channel knowledge with respect to the different channel classes and the various bandwidth. Moreover, based on the subspace analysis, we intend to verify such information to further make the channel characterizations be clearer. Furthermore, we point out that the transmission over a wide-band might not be a good idea comparing to multi-band conception.

The paper is organized as follows: Sec. II gives a brief description of the measurement environment. In Sec. III, we analyze the channel features based on the Maximum Entropy Method (MEM). In Sec. IV, we further verify the remark, obtained in the Sec. III, using a subspace analysis. In Sec. V, we present the multi-band evaluation.

II. CHANNEL SOUNDER HARDWARE

In this section, we give a simple description of the devices used in the measurements. The wide-band propagation measurements were undertaken in the 30 kHz-100 Mhz band in various indoor channel environments (country and urban, new and old, apartments and houses) and were executed by Orange Labs, Lannion [?]. The transfer function measurements were therefore carried out in the frequency domain by means of a vectorial network analyzer, as shown in the block diagram of Fig. 1.
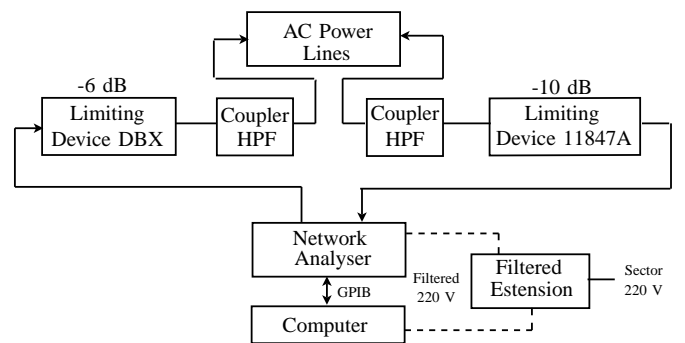
Fig. 1.   Power-line channel measurement system.

The details presenting each of these boxes can be found in [?]. After a large number of data collecting and analyzing, the indoor PLC channel can be statistically classified into 9 categories named $1-9$ classes. Further, a statistical study on the measured transfer function peaks and notches is implemented for each channel class. In turns, there come up with a PLC magnitude generator and a phase generator. In this paper, we

will analyze the channel characteristics w.r.t the various classes using these measurements.

III. Maximum Entropy Method analysis

The principle of Maximum Entropy Method (MEM) was originally used by Burg to analyze the signal spectrum based on its second-order statistics [?]. Nevertheless, this approach was further dually-applied to modelize the wireless channel supposing that the covariance channel knowledge is available [?]. In fact, when the modelling is based on measurements, the estimate of the covariance channel knowledge is always assumed to be available. Here, we aim at taking advantage of this method to investigate the indoor PLC channel characteristics. Let $\{h_i\}_{i \in \mathbf{Z}}$ be the sequence of samples at frequencies $i\delta_f$, δ_f is the frequency resolution, of the channel frequency response and, then, the spectral autocorrelation function is defined as

$$R(k) = \mathrm{E}[h_i h_{i+k}^*], \quad k = 0, \cdots, N, \quad \text{for all} \quad i \quad (1)$$

where $\mathrm{E}[\cdot]$ denotes expectation; the superscript $*$ stands for conjugate. According to Burg's theorem [?], the maximum entropy of a random process fits the N-th order Autoregressive (AR) model with its form as

$$h_i = -\sum_{k=1}^{N} a_k h_{i-k} + Z_i, \quad (2)$$

where the Z_i are i.i.d. $\sim N(0, \sigma^2)$ and $a_1, \cdots, a_N$, σ^2 are chosen to satisfy (1). The coefficients $a_1, \cdots, a_N, \sigma^2$ can be obtained by solving the Yule-Walker equations

$$
\begin{aligned}
R(0) &= -\sum_{k=1}^{N} a_k R(-k) + \sigma^2, \\
R(q) &= -\sum_{k=1}^{N} a_k R(q-k), \quad q = 1, \cdots, N.
\end{aligned}
$$

The power delay spectrum (PDS) of the N-th order AR process (2) yields

$$P(\tau) = \frac{\sigma^2}{|1 + \sum_{k=1}^{N} a_k e^{-j2\pi k\tau}|^2}, \quad (3)$$

where $\tau = \frac{\hat{\tau}}{T_s}$ is the normalized delay and $\hat{\tau}$ is the delay in seconds; T_s is the symbol duration. In practice, the spectral autocorrelation function is estimated from a finite set of N frequency measurements e.g. $[h_1^l, \cdots, h_N^l]$ over a bandwidth of $N\delta_f$ (l is the l-th channel realization). A sampled autocorrelation function yields [?]

$$\hat{R}^N(k) = \frac{1}{LN} \sum_{l=1}^{L} \sum_{i=1}^{N-k} h_i^l (h_{i+k}^l)^*, \quad k \geq 0,$$

where L is the number of channel realizations. For a given N, we estimated the autocorrelation function $\hat{R}^N(k)$, the coefficients $\hat{a}_k^N$ and the PDS $\hat{P}^N(\tau)$. As a consequence, the estimated entropy is given by

$$\hat{H}^N = \log(\pi e) + \int_{-1/2}^{1/2} \log \frac{\sigma^2}{|1 + \sum_{k=1}^{N} \hat{a}_k^N e^{-j2\pi k\tau}|^2} d\tau.$$
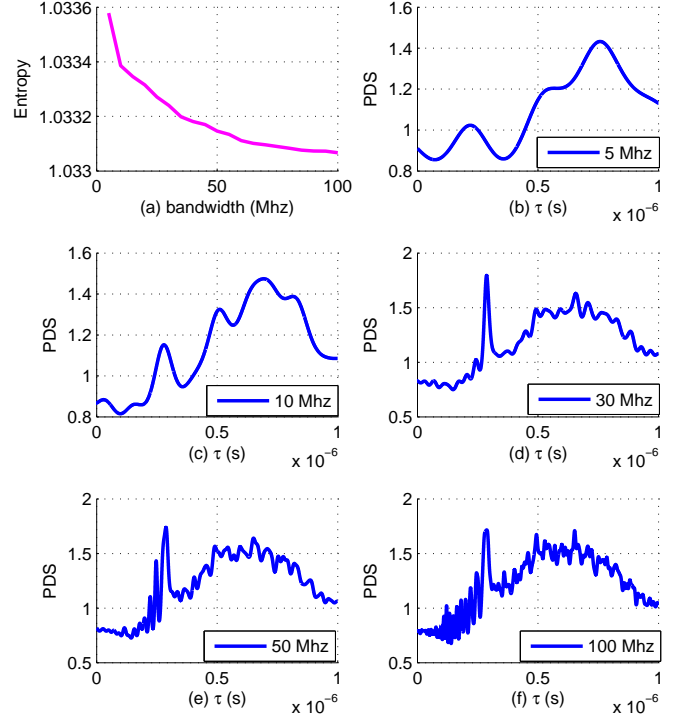
Fig. 2.   Estimated entropy and PDS for class 3.
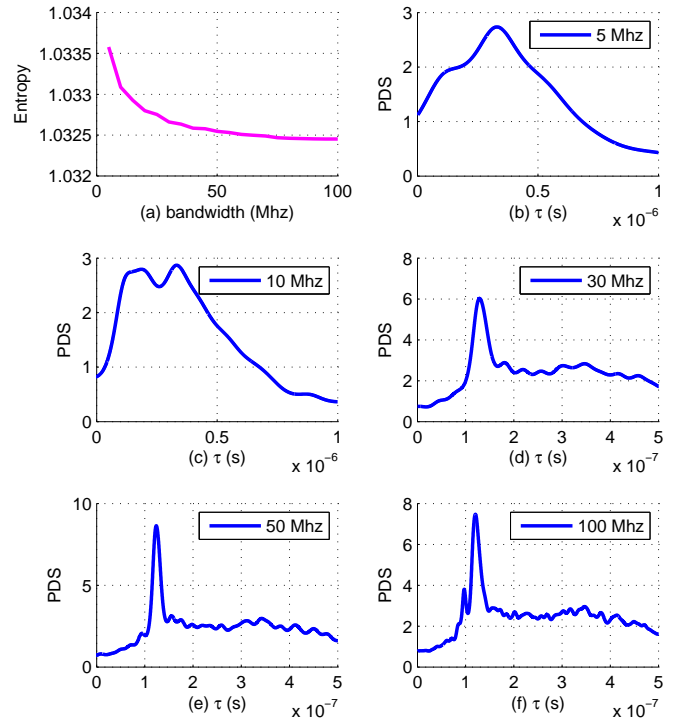
Fig. 3.   Estimated entropy and PDS for class 6.
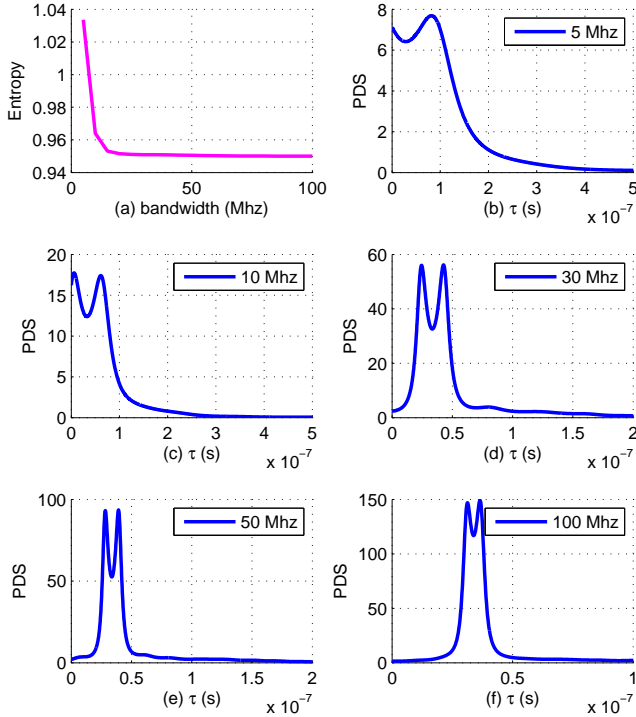
Fig. 4. Estimated entropy and PDS for class 9.

The roots of the power delay spectrum (3) determine the number of significant clusters. However, in practice, some existing roots may not be significant and they are unnecessary to model. The analysis on the $\hat{H}^N$ w.r.t N may demonstrate this.

The estimated entropy and PDS for the class $3, 6, 9$ are depicted in Fig. 2, 3 and 4, respectively. In each class, the estimated entropy is plotted versus an ascending bandwidth up to 100 Mhz. The estimated PDSs with varied bandwidth are also given in these figures (we take bandwidth of $5, 10, 30, 50, 100$ Mhz for comparison). Let us first see the entropy comparison. The entropy of the class 3 (see, Fig 2(a)) at a fixed bandwidth is higher than that of the class 6 and 9 at that bandwidth. According to Burg's saying that the higher entropy leads to a wider spectrum [?], we can therefore expect a wider PDS for the class 3 than the class 6 and 9. This inference can be easily verified by checking the estimated PDSs (the PDSs are plotted with different scales) with a fixed bandwidth (e.g. comparing Figs. 2(f), 3(f) and 4(f)). Thereby, we can reasonably deduce that the channel impulse response (CIR) of the class 3 is longer than that of the class 6 and 9 (the class 9 has the shortest CIR). It alternatively says that the frequency transfer function for the class 9 is flatter than the other classes. Thus, our first viewpoint yields that with increasing the class number, the length of the CIR tends to be a descending order and the channel with smaller class number suffers more frequency selectivity effect.

Next, we intend to investigate how does the entropy change by increasing the bandwidth for each class. In the class 3 case, we find that in the narrow-band region (say, $1 - 30$ Mhz), the entropy does not rapidly descend when we increase the bandwidth. However, for the class 9, the entropy slope appears to be quite steep in this region. That means, by augmenting the bandwidth up to 30 Mhz, the class 9 gains much more information about the channel knowledge than the class 3. But if we move to the wide-band region (i.e. beyond 30 Mhz), the entropy of the class 3 keeps descending, although again, it descends slowly. The class 9, on the contrary, shows a flat floor tendency. For this situation, it seems that, in the wide-band region, the class 9 cannot gain very much information from the wide-band but the class 3 still does. (Note that, the class 6 places somewhere in between the class 3 and 9). Actually, the estimated PDS may give the evidence to confirm this deduction. Let us see the PDS in narrow-band case (e.g. $5, 10$ Mhz) for each class. We find that from 5 to 10 Mhz, the PDS of the class 3 does not have a well described shape, but, in the class 9 case, its PDS has almost a definitive shape. When we switch to wide-band region, the PDS of the class 9 barely changed comparing to the ones in narrow-band region. However, the PDS of the class 3 has pretty much refined its shape based on the information obtained from the wide-band. Indeed, our viewpoint above can give the explanation. That is: since the class 3 has higher selectivity behavior in frequency domain, it surely needs more samples (in frequency) to estimate the model, on the contrary, the class 9 behaves more flatly in frequency, so even a small amount of samples in frequency may be enough to describe the channel. Alternatively, the estimated entropy can also confirm such explanation, i.e. since higher entropy results in a higher uncertainty for the channel knowledge, thus, a modelling for the smaller class number channels with only a small number of samples tends to be fairly hard.

On the other hand, for the channel behaving like the class 9, we usually suggest to use multi-band system instead of wide-band. Thus, we can gain more capacity from the bands. The multi-band evaluation will be discussed later on.

IV. Degree of Freedom analysis for indoor PLC channel

In the preceding section, we investigated the indoor PLC channel characteristics using a MEM approach. We find that the smaller number of PLC channel class possesses the longer delay spread and suffers worse frequency selectivity. Moreover, we remark that the channel of larger class number might be more appropriate for multi-band system. In this section, we further verify this remark by investigating the degree of freedom (DoF) for the different channel classes. Our approach, to do so, is based on the analysis of the channel subspace and the eigendecomposition of the covariance matrix, $\mathbf{K_c}$, of the samples of channel time response, which can be obtained by applying the inverse Fourier transform to the samples of the observed channel process $[h(0), \cdots, h((N - 1)\delta_f)]^T$, where the superscript ^{T} stands for the transpose operation, in the

frequency domain [**?**]. The covariance matrix of measured channel samples, $\mathbf{c}$, is written as

$$\mathbf{K_c} = \mathrm{E}\left[\mathbf{cc}^H\right] = \mathrm{E}\left[\mathbf{gg}^H\right] = \sigma^2 \mathbf{I}, \qquad (4)$$

where $\mathbf{g}$ is a vector of samples of the noise-free channel process, and $\mathbf{I}$ is the identity matrix; The superscript ^{H} denotes paraconjugate operation. Assume that the noiseless channel has length p, then the maximum-likelihood covariance matrix estimate computed from N statistically independent channel observation with length N and $p < N$ yields [**?**]

$$\mathbf{K_c}^N = \frac{1}{N}\sum_{i=1}^{N} \mathbf{c}_i \mathbf{c}_i^H. \qquad (5)$$

The covariance matrix is Hermitian positive definite. Thus, a unitary matrix $\mathbf{U_c}$ exists such that the Karhunen-Loéve (KL) expansion gives

$$\mathbf{K_c}^N = \mathbf{U_c}\boldsymbol{\Lambda_c}\mathbf{U_c}^H = \sum_{i=1}^{N} \lambda_i(\mathbf{c})\psi_i(\mathbf{c})\psi_i^H(\mathbf{c}), \quad \mathbf{U_c}^H\mathbf{U_c} = \mathbf{I}_N, \qquad (6)$$

where $\lambda_1(\mathbf{c}) \geq \lambda_2(\mathbf{c}) \geq \cdots \geq \lambda_N(\mathbf{c})$, $\psi_i(\mathbf{c})$ is the i-th column of $\mathbf{U_c}$; $\lambda_i(\mathbf{c})$ and $\psi_i(\mathbf{c})$ are the i-th eigenvalues and eigenvectors of $\mathbf{K_c}^N$, respectively. Decomposing (5) into principal and noise components yields

$$\mathbf{U}_{s,\mathbf{c}} = [\psi_1(\mathbf{c}),\cdots,\psi_L(\mathbf{c})],$$
$$\lambda_1(\mathbf{c}) \geq \cdots \geq \lambda_L(\mathbf{c}),$$
$$\mathbf{U}_{n,\mathbf{c}} = [\psi_{L+1}(\mathbf{c}),\cdots,\psi_N(\mathbf{c})],$$
$$\lambda_{L+1}(\mathbf{c}) \geq \cdots \geq \lambda_N(\mathbf{c}),$$

where $\mathbf{U}_{s,\mathbf{c}} \perp \mathbf{U}_{n,\mathbf{c}}$. $\mathbf{U}_{s,\mathbf{c}}$ defines the subspace containing both signal and noise components, whereas $\mathbf{U}_{n,\mathbf{c}}$ denotes the noise only subspace. L is the number of significant eigenvalues which also represents the channel DoFs [**?**], in the sense that any set of observations can be characterized by a set of approximately L independent random variables which excite L modes (their corresponding eigenvectors).

The empirical results are shown as below. In our simulation, the frequency resolution was 100 Khz/sample. We first see the Power Delay Profile (PDP) curves which are depicted in Fig. 5. It confirms our viewpoint presented in the preceding section. In Figs. 6, 7 and 8, we plot, for different classes, the fraction of the captured energy for M considered eigenvalues defined by $E_M = \sum_{i=1}^{M} \lambda_i(\mathbf{c})/\sum_{i=1}^{N} \lambda_i(\mathbf{c})$, where N is the total number of eigenvalues. We observe that, for the class 3 and 6, the majority of the channel energy (say, 90%), in narrower bandwidth case, is confined in a small number of significant eigenvalues; whereas in the wide band-width case, the channel energy is spread over a large number of the eigenvalues. However, this situation is a bit different for large class number (e.g. class 9). In Fig. 8, the solid cures represent the bandwidth less than 50 Mhz and for the ones beyond 50 Mhz are plotted in dash lines. We find that when the bandwidth is less than 50 Mhz, the curves have a similar disposition as in the class 3 and 6 cases. However, when the bandwidth is beyond 50 Mhz, the curves are displaying by an
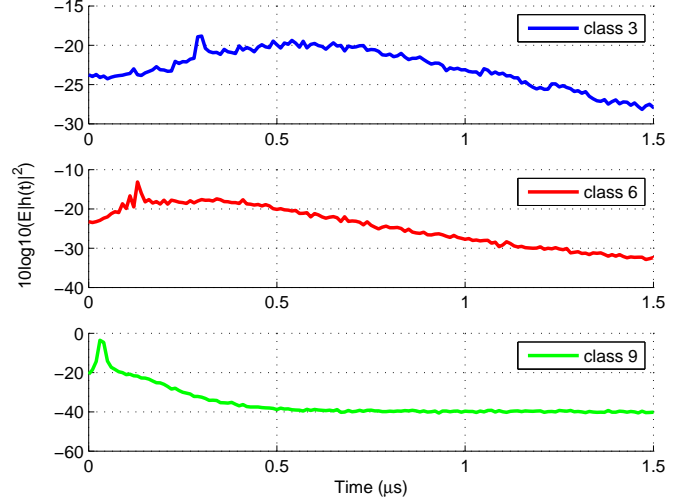
Fig. 5.   Power Delay Profile in variant class case.
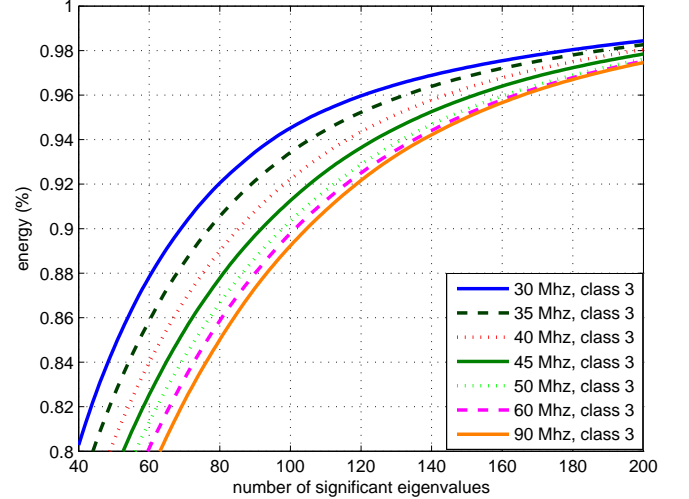
Fig. 6.   Fraction of the captured energy versus the number of significant eigenvalues in class 3 case.

opposite order. Furthermore, for the class 9, the majority of the channel energy concentrates on the very beginning number of eigenvalues, e.g., the first 5 eigenvalues contain almost 84% channel energy for all bandwidth cases. If we further zoom in the zone A (see, Fig. 9), it seems that the first extracted DoFs, with smaller bandwidth cases, have the smaller energy compared to the others extracted with larger bandwidth.

Fig. 10, plotted for 95% captured energy, shows that the number of significant eigenvalues increases with the channel bandwidth. We see that, for the class 3, the increase is linear until bandwidth is less than 50 Mhz, where a saturation effect begins to occur. This critical bandwidth can be actually seen as the threshold, below which, the signal bandwidth does not effectively provide sufficient resolution to resolve
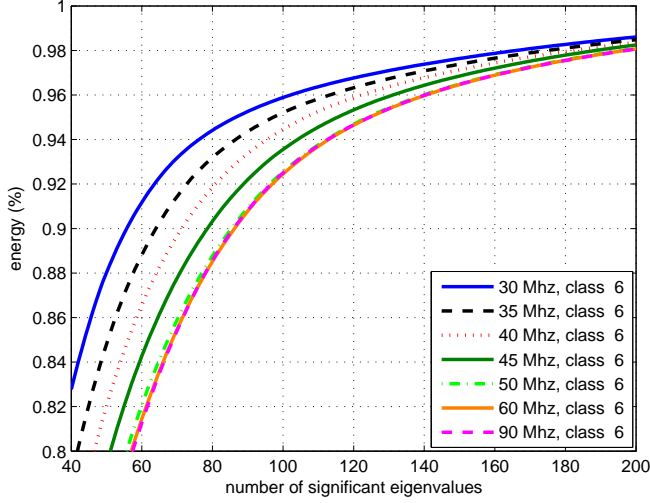
Fig. 7. Fraction of the captured energy versus the number of significant eigenvalues in class 6 case.
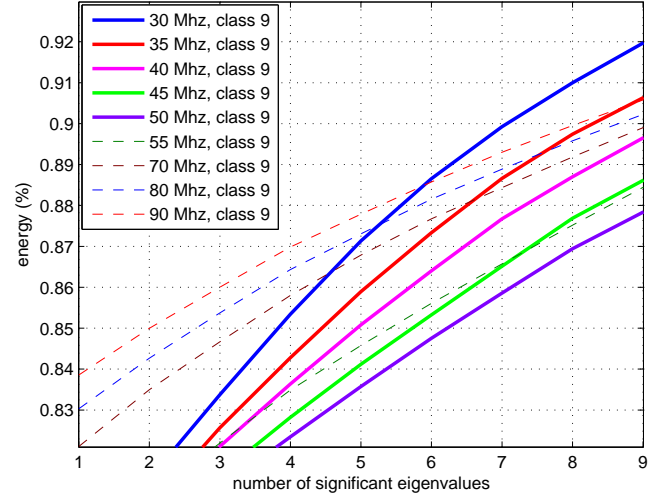
Fig. 9. A zoomed version of Fig. 8.
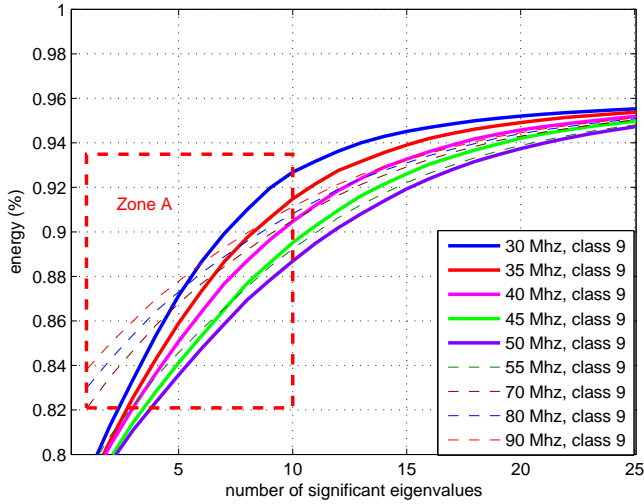
Fig. 8. Fraction of the captured energy versus the number of significant eigenvalues in class 9 case.
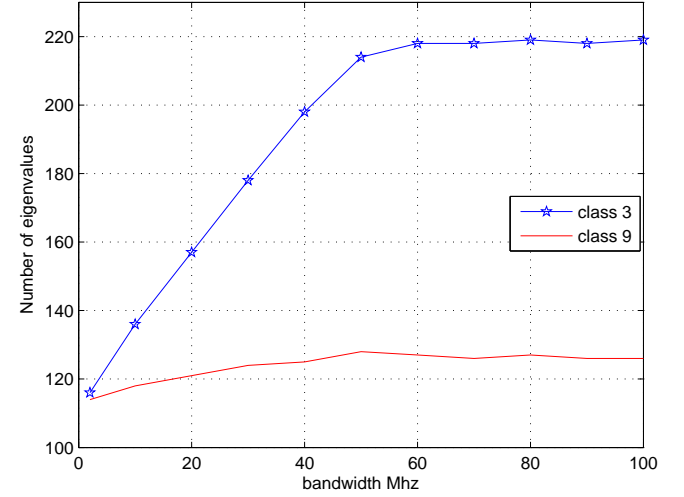
Fig. 10. Evolution number of the eigenvalue for variant class case.

all eigenvalues, or the complete number of multi-path components. Beyond this point, on the other hand, the channel is degenerated in the sense that all the paths can be resolved. Therefore, it will be not necessary to continue enlarging the bandwidth. It is obvious that the class 9 begins to saturate at a pretty smaller bandwidth threshold (around 20 Mhz) and the number of DoFs for the class 9 is much less than that of the class 3. Thus, this can prove our remark that for larger class number, multi-band system is more appropriate.

V. MULTI-BANDS EVALUATION

In the section III, we remarked that the larger class number PLC channel is more appropriate for multi-band system based on the entropy analysis. Then, in the section IV, the subspace

analysis gave us an evidence that the number of DoFs for the larger class number is much less than the smaller class number and, with increasing the bandwidth, the DoF cannot be significantly increased for the larger class number. The conclusions of the previous two sections are actually consistent with each other. Finally, in this section, we will numerically evaluate our remark. For the sake of simplicity, we still choose these three classes i.e. class 3 6 and 9 for comparison. In what follows, we will calculate the channel capacity of using multi-band and wide-band for each class. The capacity calculation is based on the Shannon's capacity formula and for the same reference noise and power spectral density (PSD) emission mask [?]. The calculation parameters are: Carrier width ($\delta_f = 100$ Khz); Transmitted PSD ($P_e = -50$ dBm/Hz); White noise PSD ($P_b = -140$ dBm/Hz); Number of the carriers N is subject

to the bandwidth (i.e. wide-band: $1 - 90$ Mhz; multi-band: $1 - 30$, $30 - 60$, $60 - 90$ Mhz). The capacity C formula for one measurement is given by

$$C = \Delta f \sum_{i=1}^{N} \log_2 \left(1 + \frac{P_e \cdot |h(i\delta_f)|^2}{P_b} \right) \text{(bis/s)} \quad (7)$$

The results are layout in the Table. **??**, where the capacity is averaged over a large set of measurements. The results proved our remark, i.e. the capacity improvements for the class 9, 6 and 3, using multi-band instead of wide-band, are 5.7, 4.6 and 3.3 Mbits/s, respectively. This improvement can also be called multi-band gain.

TABLE I
CAPACITY COMPARISON.

Capacity (Gbits/s)	class 9	class 6	class 3
C_{1-30}	0.8371	0.6952	0.5329
C_{30-60}	0.8548	0.6873	0.4931
C_{60-90}	0.8245	0.6335	0.4459
C_{1-90}	2.5107	2.0115	1.4686

VI. CONCLUSION

In this paper, we analyzed the indoor PLC channel characteristics from an information theory point of view for different PLC classes. We first used the MEM approach to estimate the entropy and PDS for each channel class. It turned out that the small number class channels have relatively longer delay spread than the larger number class ones. In addition, the small number class channels behave more selectivity in frequency. Moreover, from the hint of entropy analysis, we remarked that larger number class channels are more appropriate for multi-band system. Further, an eigendecomposition analysis was applied to investigate the DoF for each class. It revealed that the DoF of small number class channels are higher than that of larger number class ones. Meanwhile, we observed that, with increasing the band-width, the speed of DoF tending to a saturation for larger number class is faster than the smaller

number classes, which further verified our remark. Finally, we evaluated the multi-band benefits in terms of the channel capacity to eventually prove our remark.

REFERENCES

[1] *HomePlug AV Specification*, Version 1.0.05, Oct 2005.
[2] V. Degardin, M. Lienard, A. Zeddam, F. Gauthier, and P. Degauque, "Classification and characterization of impulsive noise on indoor power lines used for data communications," *IEEE Trans. Consum. Electron.*, vol. 48, no. 4, pp. 913–918, Nov 2002.
[3] T. Esmailian, F. R. Kschischang, and P. G. Gulak, "In-building power lines as high-speed communication channels: Channnel characterization and a test channel ensemble," *Int. J. Commun. Syst.*, 2003.
[4] H. Pilipps, "Development of a statistical model for powerline communication channels," in *ISPLC*, 2000.
[5] M. Tlich, A. Zeddam, F. Moulin, and F. Gauthier, "Indoor Power-line Communications Channel Characterization Up to 100 Mhz-Part I: One-Parameter Deterministic Model," *IEEE Transactions on Power Delivery*, vol. 23, pp. 1392–1401, 2008.
[6] M. Tlich, A. Zeddam, F. Moulin, and F. Gauthier, "Indoor Power-line Communications Channel Characterization Up to 100 Mhz-Part II: Time-Frequency Aanalysis," *IEEE Transactions on Power Delivery*, vol. 23, pp. 1402–1409, 2008.
[7] J. P. Burg, *Maximum Entropy Spectral Analysis*, Ph.D. dissertation, Stanford University, 1975.
[8] R. L. de Lacerda, A. Menouni, M. Debbah, and B. H. Fleury, "A Maximum Entropy Approach To UWB channel modelling," in *ICASSP*, 2005.
[9] T. M. Cover and J. A. Thomas, *Elements of Information Theory*, Wiley, 2006.
[10] J. G. Proakis and D. G. Manolakis, *Digital Signal Processing: Principle, Algorithms, and Applications*, Prentice-Hall, 1996.
[11] R. Bultitude, R. Hahn, and R. Davies, "Propagation considerations for the design of indoor broadband communications system at EHF," *IEEE Trans. Vehic. Technol.*, vol. 47, no. 1, pp. 23–30, Feb 1998.
[12] T. W. Anderson, *An Introduction to Multivariate Statistical Analysis*, Wiley, 1984.
[13] M. Wax and T. Kailath, "Detection of signals by information theoretic criteria," *IEEE Trans. on Acoust. Signal Speech Process.*, vol. 33, no. 2, pp. 387–392, 1985.